Large-Scale Dendrimer-Based Uneven Nanopatterns for the Study of Local RGD Density Effects on Cell Adhesion

Anna Lagunas,[1,2] Albert G. Castaño,[2,1] Juan M. Artés,[2,3,†] Yolanda Vida,[4,5] Daniel Collado,[4,5] Ezequiel Pérez-Inestrosa,[4,5] Pau Gorostiza,[2,1,6] Silvia Claros,[7,1] José A. Andrades,[7,1] and Josep Samitier[1,2,8]

[1]Networking Biomedical Research Center in Bioengineering, Biomaterials and Nanomedicine (CIBER-BBN)

[2]Institute for Bioengineering of Catalonia (IBEC), Baldiri-Reixac 15-21, Barcelona 08028 Spain

[3]Physical Chemistry Department, University of Barcelona (UB), Martí i Franquès 1-11, Barcelona 08028 Spain

[4]Andalusian Centre for Nanomedicine and Biotechnology (BIONAND), Severo Ochoa 35, Málaga 29590 Spain

[5]Organic Chemistry Department, University of Málaga (UMA), Campus Teatinos, Málaga 29071 Spain

[6]Institució Catalana de Recerca i Estudis Avançats (ICREA)

[7]Cell Biology, Genetics and Physiology Department, University of Málaga (UMA), Campus Teatinos, Málaga 29071 Spain

[8]Electronics Department, University of Barcelona (UB), Martí i Franquès 1-11, Barcelona 08028 Spain

[†]Present address: Electrical and Computer Engineering department, University of California Davis, 95616 Davis CA

ABSTRACT

Cell adhesion process is governed by the nanoscale arrangement of the extracellular matrix (ECM), being more affected from local than from global concentration of cell adhesive ligands. Dendrimers grafted on surfaces showed the benefits of the local increase in concentration provided by the dendritic configuration, in many cell-based studies; although the lack of any surface characterization has limited a direct correlation with dendrimer disposition and cell response. In order to establish a proper correlation, some control in dendrimer surface deposition is desirable. Here, dendrimer nanopatterning is applied to address arginine-glycine-aspartic acid (RGD) density effects on cell adhesion. Nanopatterned surfaces were fully characterized by atomic force microscopy (AFM), scanning tunneling microscopy (STM) and X-ray photoelectron spectroscopy (XPS), showing that tunable distributions of cell-adhesive ligands on the surface are obtained as a function of the initial dendrimer bulk concentration. Cell experiments showed a clear correlation with dendrimer surface layout: substrates presenting regions of high local ligand density resulted in a higher percentage of adhered cells and a higher degree of maturation of focal adhesions (FAs). Therefore, dendrimer nanopatterning is presented as a suitable and controlled approach to address the effect of local ligand density in cell response. Moreover, due to the easy modification of dendrimer peripheral groups, dendrimer nanopatterning can be further extended to other ECM ligands with density effects on cells.

KEYWORDS

Dendrimer, RGD, AFM, STM, cell adhesion, focal adhesions.

Introduction

For an adherent cell exposed to a surface, the early steps of cell-surface interaction are mediated mainly by integrins [1,2]. These molecules are heterodimeric transmembrane proteins that recognize and become activated by certain aminoacid sequences present in the extracellular matrix (ECM) proteins. Upon integrin activation, cytoplasmic protein recruitment leads to the formation of transient focal complexes at the cell periphery. These complexes can disassemble or eventually evolve into mature focal adhesions (FAs) that link to the cytoskeleton and mediate strong adhesion to the substrate [3]. Like many cell membrane receptors that aggregate into clusters to produce sustained signaling effects [4], integrin clustering is required for transient focal complexes to grow into mature FAs. The clustering of integrins and thus cell adhesion is governed mainly by the physiological arrangement of the ECM [5-7]. Experimental evidence of ECM organization at the nanoscale steered the production of synthetic nanopatterned surfaces directed towards identifying the geometric cues that initiate and guide cell adhesion [8,9]. Nanopatterning of ECM motives for the study of cell-surface interactions at the nanoscale highlighted the relevance of ECM ligand presentation to cells on receptor clustering, with cell-adhesion being favored more from local than from global ligand concentrations [10-12]. In that sense, dendritic molecules presenting a highly branched and easily tunable size and chemical structure emerged as ideal scaffolds for the construction of surfaces devoted to the study of ligand density effects on cells. Dendrimers grafted onto surfaces, and in situ modified through their peripheral groups for specific cell interactions [13-15], showed the benefits of the local increase in ligand density in cell adhesion [16,17], morphology [18,19], and migration events [20]. Griffith and co-workers presented the first systematic study on the effects of ECM ligand clustering on cell adhesion and migration [21]. They used star polyethylene oxide tethers modified with the adhesion ligand YGRGD to demonstrate that cell motility can be varied by regulating nanoscale ligand density, with a clustered presentation enhancing cell migration speeds. The main drawback in this study is the lack of any surface characterization on ligand disposition. In order to facilitate the correlation between ligand surface disposition and cell response, it is desirable to exert some degree of control on the deposition of dendrimers on the surface. For sufficient low-charged surfaces, dendrimers can be patterned on the

nanometer scale in a liquid-like order with large and well-defined spacing at low ionic strengths [22]. Dendrimer adsorption onto surfaces has been extensively studied and addressed through different surface characterization techniques such as fourier transform infrared-external reflection spectroscopy (FTIR-ERS) and ellipsometry [23], atomic force microscopy (AFM) [24,25], and scanning tunneling microscope (STM) [26] among others. Here, dendrimer nanopatterning is applied for the first time to create uneven distributions of the cell adhesive motive arginine-glycine-aspartic acid (RGD) to address nanoscale ligand density effects on cell adhesion. In contrast with other nanopatterning techniques [8], due to its simplicity, dendrimer nanopatterning can be straightforwardly scaled up to large surface areas, therefore being fully compatible with cell culture protocols. Surfaces derived from RGD-tailored dendrimers nanopatterning were fully characterized by AFM, STM and x-ray photoelectron spectroscopy (XPS). Surface analysis showed that tunable local ligand densities were obtained as a function of the initial bulk concentration. Cell experiments showed that dendrimer nanopatterns sustained cell adhesion and were preferential sites to establish the first cell-substrate interactions. Results demonstrated that dendrimers can mediate integrin clustering at high surface local RGD densities, leading to the formation of mature FAs. Dendrimer nanopatterning is therefore presented as a suitable approach for the study of RGD presentation on cell adhesion process and, due to the easy modification of the peripheral chemical groups in dendrimers, it can be further extended to other ECM ligands with clustering effects on cells.

1. Experimental

1.1 Dendrimer nanopatterning on Au(111) substrates

Deionized water (18 MΩ cm-1 Milli-Q, Millipore) was used to prepare all solutions and for rinsing samples. Surface nano-patterning was conducted as previously described [22,26] by immersing flame-annealed 1.4x1.1 cm Au(111) on mica substrates (Spi Supplies) on aqueous solutions of the RGD-tailored dendrimer RGD-Cys-D1 (see Electronic Supplementary Material (ESM) for RGD-Cys-D1 synthesis details) for 16 h (pH = 5.6, T = 293K). All solutions were sonicated and filtered (MILLEX RB Filter Sterile, Millipore) previously. Dendrimer stock solution was used within 6 months of preparation. RGD-Cys-D1 nanopatterning was followed by copious rinsing with water and drying with argon.

1.2 Patterning imaging and data analysis

Nanopatterned substrates were imaged by AFM in a Dimension 3100 AFM instrument (Veeco Instruments) operated in tapping mode in air. Silicon AFM probes (Budget Sensors) with a spring constant k = 40 N/m and a resonant frequency ν = 300 kHz were used. Image thresholds were obtained manually from AFM height images and processed with Image J 1.44p freeware (http://imagej.nih.gov/ij). Particle positions were used to obtain minimum inter-particle distances (d_{min}) using a custom-generated MATLAB code (The MATHWORKS, Inc.; ESM). dmin values were analyzed with OriginPro 8.5.0 SR1 (OriginLab Corp.). Mean minimum inter-particle spacing was obtained from fitting the resulting dmin distributions to a lognormal model (Figure S2 in ESM). At least four images were computed per sample in two independent experiments. Probability contour plots for d_{min} were constructed from d_{min} values for each particle position and plotted in zeta using an adapted MATLAB code from http://www.eng.cam.ac.uk/help/tpl/programs/Matlab/matlabbyexample/ (see ESM). Threshold images were superimposed for clarity. STM measurements in air were carried out in a PicoSPM microscope (Molecular Imaging) controlled by Dulcinea electronics (Nanotec Electronica) using WSxM 4.0 software [27]. Etched Pt0.8:Ir0.2 probes with a diameter of 0.25 mm were used (Agilent Technologies).

1.3 Preparation of control substrates

Homogeneously modified substrates were prepared by immersing flame-annealed Au(111) substrates in a solution of RGD-PEG-SH and triethylene glycol mono-11-mercaptoundecyl ether (PEG-SH) from Sigma-Aldrich at a 1:100 molar ratio in 96% ethanol (Panreac) for 16 h at room temperature. RGD-PEG-SH was kindly supplied by Prof. F. Albericio's group at the Institute for Research in Biomedicine (IRB, Barcelona, Spain) [28]. Polyethylene glycol passivated substrates were prepared by immersion of flame-annealed Au(111) substrates in a 1 mM solution of PEG-SH in 96% ethanol for 16 h at room temperature. After incubation, substrates were thoroughly washed in ethanol and dried with argon. All solutions were sonicated and filtered prior to substrate incubation.

1.4 Cell culture and fluorescent staining

All steps, including work on the cell culture, were performed in a sterile laminar flow hood, and only sterile materials, solutions and techniques were used. All cell culture reagents were purchased from Invitrogen S. A. NIH 3T3 mouse embryonic fibroblasts from passages 8-9 were cultured at 37 ºC and 10% CO2 in Dulbecco's Modified Eagle Medium (D-MEM) liquid high glucose supplemented with 10% FBS, 1% L-glutamine,

1% penicillin-streptomycin and 1% sodium pyruvate. The medium was exchanged every second day. Nanopatterned surfaces were incubated in PBS for 15 min prior to use. After trypsinization, cells were seeded at a cell density of 4000 cells/cm2 in D-MEM liquid high glucose supplemented with 1% FBS 1% L-glutamine, 1% penicillin-streptomycin and 1% sodium pyruvate, and incubated for 4.5 h at 37 ºC and 10% CO2. Control experiments with homogeneously modified, polyethylene glycol-passivated and bare Au(111) substrates were performed. Post-incubation, non-adherent cells were removed by a gentle wash with PBS and the attached cells were fixed with a 10% neutral buffered formalin solution from Sigma-Aldrich for 20 min and then washed with PBS. The remaining free aldehyde groups were blocked with 50 mM amonium chloride (NH4Cl) from Merk Sharp & Dohme in PBS for 20 min at room temperature. Afterwards, samples were washed with PBS, and cells were permeabilized with a solution of 0.1% saponin (Fluka) in 1% BSA from Sigma-Aldrich in PBS for 10 min at room temperature. To visualize focal adhesions (FAs) and cell cytoskeleton actin fibers, rabbit monoclonal anti-paxillin [Y113] (Abcam) diluted 1:200 and phalloidin-FITC (0.5 mg/mL) from Sigma-Aldrich diluted 1:500 in 1% BSA in PBS were added and cells were incubated for 1 h at room temperature. Cells were washed with PBS and incubated for 1 h at room temperature with the secondary antibody goat anti-rabbit IgG (H+L) ALEXA FLUOR 568 (2 mg/ml) and Hoechst (10 mg/ml) for cell nuclei staining, both from Invitrogen S. A. and diluted 1:1000 in 1% BSA in PBS. After incubation, cells were washed with PBS, and samples mounted with FLUOROMOUNT aqueous mounting medium (Sigma-Aldrich).

1.5 Cell imaging and data analysis

Cells were imaged by fluorescence microscopy with an Eclipse E1000 upright microscope (Nikon) equipped with a CCD camera and working with a green excitation G-2A long-pass emission filter for paxillin visualization, a FITC filter for actin fibers and a UV emission filter for cell nuclei. In fluorescent micrographs, the number of adhered cells was identified by stained nuclei, and paxillin immunostaining was used to determine the size and number of FAs. ImageJ freeware image analysis was used for quantification. In cell adhesion experiments, 15 images with the 10X objective were computed per sample. For FA quantification, images corresponding to paxillin staining were converted to 8-bit files. The background was removed (rolling bar radius 10), and the resulting images were converted to binary by setting a threshold. Threshold values were determined empirically, and FAs were considered from 1 μm2. A minimum of 30 cells per sample were analyzed.

1.6 Statistics

At least three independent experiments were performed per sample with different cell batches. Quantitative data are displayed, showing average and standard error of the mean. Significant differences were judged using Student T-test with a t value of less than 0.05 considered statistically significant.

2. Results and Discussion

2.1 Nanopatterning of RGD-Cys-D1 dendrimers and characterization of surface disposition

Water-soluble polyamidoamine (PAMAM) G1 dendrimers were chosen to construct nanoscale cell adhesive clusters. The use of low generation PAMAM dendrimers (less than G5) is preferred since they have proven more biocompatible and less immunogenic than high generation ones [29]. In order to make dendrimers compatible with cell-based experiments and trigger cell adhesion, the primary amine surface groups on the outermost layer of the PAMAM dendrimers were functionalized with the cell adhesive linear RGD polypeptide (see ESM). PAMAM dendrimer-RGD peptide conjugates were synthesized as depicted in Scheme 1.

The maleimido-functionalized generation-1 PAMAM dendrimer was reacted chemoselectively with a single cysteine (Cys) at the C-terminus of RGD, by adapting a previously described procedure [30,31], to generate RGD-Cys-D1, which assembles eight copies of the RGD peptide.

RGD-Cys-D1 dendrimers were patterned onto flame annealed Au(111) substrates by immersion in aqueous solutions of RGD-Cys-D1 of 10-8- 10-2% w/w concentration for 16 h (pH = 5.6, and T = 293K). The resulting, dendrimer nanopatterns were imaged by AFM and STM in air. For low bulk concentrations, up to 10-5 % w/w, isolated dendrimers of 4-5 nm in diameter can be observed (Fig. 1).

Minimum interparticle distances (dmin) obtained from AFM image thresholds (Fig. 2 and Fig. S2 in the ESM) were used to characterize the local density on the surface. Since dendrimers are unevenly distributed, individual inter-dendrimer spacing or even the mean inter-dendrimer spacing values calculated here from dmin distribution fittings (Fig. 2(b)) are not suitable to describe the local density [32]. Therefore, dmin values obtained for each particle position are plotted in zeta to construct the probability contour plots for dmin shown in Fig. 2(c) where high density RGD regions are highlighted. As shown in Figure 2(c), slight variations in the mean interligand spacing caused an abrupt increase of denser

ligand regions. If we consider RGD-Cys-D1 dendrimers separated less than 70 nm, the percentage of dense areas increase from 7%, for surfaces derived from 10-8% w/w bulk concentration, to 79%, for surfaces derived from 10-5% w/w bulk concentration.

Patterning from high bulk concentrations, 10-2% w/w for 16 h, resulted in dendrimer aggregation. AFM images (Fig. 3(a)) showed the presence of elongated structures with an estimated average size of 650 nm2 (Fig. S3). High magnification images taken by means of scanning tunneling microscope (STM) revealed that these structures contained dendrimers assembled in a close-packed configuration (Fig. 3(b)). In order to elucidate whether aggregation occurred in solution or was a result of a surface-induced reorganization process, zeta potential was measured in the initial bulk RGD-Cys-D1 dendrimer solutions (Fig. S4 in the ESM). A zeta potential of -3.03 mV was recorded for the 10-2% w/w bulk concentration, indicating that for such high initial concentration, solution instability may lead to dendrimer aggregation and the subsequent deposition of the formed aggregates on the surface. The dmin probability contour plot (Fig. 3(d)) constructed from the threshold image in Fig. 3(c), showed that aggregation not only caused an increase of the local RGD density as expected but also increased the heterogeneity of the samples in terms of ligand distribution, if compared with nanopatterned surfaces from lower bulk concentrations.

2.2 Cell adhesion on dendrimer nanopatterns

Since the diameter of integrins in the cell membrane is around 10 nm [33] each dendrimer of 4-5 nm in diameter, although providing up to eight copies of the cell-adhesive RGD ligand, resulted in a single site for integrin binding [35]. Using dendrimer nanopatterning, a set of substrates of unevenly distributed RGD molecules with tunable local ligand density was obtained. Cell adhesion experiments were performed with NIH 3T3 mouse embryonic fibroblasts seeded at 4000 cells/cm2 for 4.5 h. Serum starvation conditions were maintained at 1% of fetal bovine serum during the experiment in order to highlight the effect of the substrate [21]. Fluorescent micrographs of adhered cells on the samples were taken after cell fixation and nuclei staining (Fig. 4a). In this case, ready-to-use substrates were obtained, with no further passivation step required, as demonstrated by the percentage of adhered cells obtained for the negative controls (bare Au(111) and polyethylene glycol (PEG-SH) passivated Au(111) substrates; Fig. 4(b)). The low percentage of adhered cells observed in Au(111) substrates can be attributed to the well-known gold-induced protein denaturation effect [35]. Therefore, cell interactions with the nanopatterned surfaces could be attributed solely to RGD-Cys-D1-cell receptor

interactions, without any passivation step that can mask the specific influence of the patterns on cell guidance [36].The percentage of adhered cells obtained from a bulk concentration of 10-8% w/w, which was lower than of the negative controls, confirm that dendrimers are preferential sites to establish the first cell-substrate interactions, and pointed out that RGD clustering effect when provided solely by the dendritic conformation is in this case, not enough to reach high percentages of cell adhesion. This is in agreement with previous reports suggesting that a coverage limit of high density ligand regions is necessary in order to generate a sufficient cell response [11,21,38]. As the bulk concentration increased, the percentage of seeded cells adhered to the substrate after 4.5 h of incubation increased to 80% for a bulk concentration of 10-5% w/w. Similar adhesion was obtained when dendrimers were presented as high density aggregates on the surface. In both cases statistical analysis showed that adhesion was significantly higher than in the homogeneously modified RGD-PEG-SH substrates (Fig. 4(b)). Since this finding could be attributed to an effect of global ligand density, we measured the elemental composition of the surface by XPS (see ESM). The atomic percentage of sulfur directly correlates with the number of RGD molecules, which differed between dendrimers and homogeneous films. The sulfur/gold ratio was found to be very similar for substrates derived from 10-5 and 10-2% bulk concentrations, resulting in 0.04±0.02 and 0.03±0.02, respectively; while much higher values were found for homogeneous surfaces, with a sulfur/gold ratio of 0.20±0.03. These observations indicate that uneven distributions of RGD obtained through RGD-Cys-D1 dendrimer nanopatterning sustain cell adhesion more efficiently than the corresponding homogeneous surfaces and highlight the relevance of local ligand density.

2.3 RGD-Cys-D1 nanopattern influence on FA formation and maturation

Since cell-matrix junctions are strongly influenced by local ligand density [12], we examined FA formation. The signal transduction adaptor protein paxillin, which is involved in FA formation from its early stages [38] was fluorescently labeled and monitored at high magnification (Figure 5a). No mature FAs developed below a bulk concentration of 2.5 10-8% w/w (Figure 5b). This is in agreement with results reported by Cavalcanti-Adam et al. [39], who found that FA dynamics is significantly delayed in overlarge inter-ligand spacing. Here, the absence of high density RGD regions in surfaces produced from bulk concentrations below 2.5 10-8% w/w. In such surfaces, the weak cell to surface interaction may favor easy cell detachment which can also contribute to the low percentage of adhered cells obtained (Fig. 4). Accordingly, an increase of bulk

concentration to 10-5% w/w, and hence an increase of local RGD density, increased the number of mature FAs. Substrates derived from 10-2% w/w bulk concentration rendering high density dendrimer aggregates resulted in a reduced number of FAs per cell compared to the number achieved from 10-5% w/w, but much larger FA areas. XPS results (sulfur/gold ratio of 0.04±0.02, 0.03±0.02 for 10-5 and 10-2% w/w bulk concentrations, respectively) showed that samples derived from 10-5 and 10-2% w/w bulk concentrations presented a similar amount of RGD on their surfaces. However, the area covered with high surface particle density ($d < 70$ nm) is very different in both cases. Therefore, the observed cell behavior should be due to the RGD local distribution in each case. With fewer cell adhesive anchor points, 10-2% bulk concentration derived surfaces made cells develop a lower number of FAs than in 10-5% w/w bulk concentration derived ones but, as predicted by Cavalcanti-Adam et al. [39], the increased local ligand density when aggregation occurs, caused FA maturation to be favored for 10-2% w/w vs. 10-5% w/w surfaces for the same period of time. These results are also supported by theoretical studies on integrin-ligand binding performed by Irvine et al. [40] which revealed that an increase in local ligand density enhances ligand-receptor affinity of neighboring integrins, thus favoring receptor clustering and reinforcing cell adhesion. In addition, Comisar et al. [41], using an integrin binding/clustering model, obtained that integrin cluster size is increased with increasing RGD distribution heterogeneity.

3. Conclusions

Dendrimer nanopatterning approach is presented to address RGD local density effects on cell adhesion. To this end, PAMAM G1 dendrimers had been chemically modified with the cell adhesive RGD peptide, in a way that each dendrimer assembled eight copies of RGD, and patterned on Au(111) substrates. AFM and STM surface analysis showed that RGD-tailored dendrimers are unevenly distributed on the surface and that tunable local RGD densities were obtained as a function of the initial bulk concentration. Probability contour plots for the minimum interparticle distance (dmin) were constructed from AFM images to visualize the surface high density RGD regions. Surface imaging also showed that dendrimer aggregate deposition took place at high initial bulk concentrations (10-2% w/w) as a result of solution instability. Cell adhesion experiments demonstrate that dendrimer-based nanopatterns sustained cell adhesion, and provided cell guidance for the first cell to substrate interactions. Dendrimers assist FA assembly and maturation at high local RGD surface densities. Our results point out the relevance of surface local ligand

density particularly in the case of dendrimer aggregates. If compared to 10-5% bulk concentration, with a similar value of surface ligand density, the higher degree of segregation in 10-2% derived surfaces, resulted in fewer but more mature FAs.

In conclusion, dendrimer nanopatterning has been successfully applied to the study of surface RGD presentation on cell adhesion studies, which were supported with an in detail surface characterization. Moreover, the versatility introduced by dendrimers which include a facile chemical modification of their peripheral groups and an easy tunable size, makes dendrimer nanopatterning suitable to be extended to the study of other ECM ligands with clustering effects on cells.

Acknowledgements

Authors thank Professor A. Hari Reddi for fruitful discussions and M. López for help in STM measurements. Authors also thank M. Sanmartí for its help in Zeta potential measurements. This work was supported by Centro de Investigación Biomédica en Red en Bioingeniería, Biomateriales y Nanomedicina (CIBER-BBN), Spain; the Nanobioengineering group at the Institute for Bioengineering of Catalonia (IBEC) receives support from the Commission for Universities and Research of the Department of Innovation, Universities and Enterprise of the Generalitat de Catalunya (2009 SGR 505). In addition, research leading to these results received support from the Spanish Ministry of Science and Education; Ministry of Economy and Competitiveness (Red TerCel; FIS PI10/02529); the Andalusian Government (P07-CVI-2781, PAIDI BIO-217, PI-0729-2010); Fundación Botín, Santander, Spain; CICYT (CTQ2009-07758; CTQ2010-20303); Commission for Universities and Research of the Department of Innovation, Universities and Enterprise of the Generalitat de Catalunya (2009 SGR 505).

Electronic Supplementary Material: further details of the synthesis and characterization of RGD-Cys-D1 dendrimers, detailed MATLAB code for dmin calculation and the corresponding probability contour plots construction, dmin calculation and cluster size estimation from AFM images and Zeta potential measurements and detailed XPS experimental are available in the online version of this article.

References

[1] Mager, D. M.; LaPointe, V.; Stevens, M. M. Exploring and Exploiting Chemistry at the Cell Surface. *Nat. Chem.* **2011**, *3*, 582-589.

[2] Geiger, B.; Spatz, J. P.; Bershadsky, A. D. Environmental Sensing Through Focal Adhesions. *Nat. Rev. Mol. Cell Biol*. **2009**, *10*, 21-33.

[3] Geiger, B.; Bershadsky, A.; Pankov, R.; Yamada, K. Transmembrane Extracellular Matrix–Cytoskeleton Crosstalk. *Nat. Rev. Mol. Cell Biol*. **2001**, *2*, 793-804.

[4] Vogel, V.; Sheetz, M. Local Force and Geometry Sensing Regulate Cell Functions. *Nat. Rev. Mol. Cell Biol*. **2006**, 7, 265-275.

[5] Smith, M. L.; Gourdon, D.; Little, W. C.; Kubow, K. E., Eguiluz, R. A.; Luna-Morris, S.; Vogel, V. Force-Induced Unfolding of Fibronectin in the Extracellular Matrix of Living Cells. *PLoS Biol.* **2007**, *5*, 2243-2254.

[6] Jiang, F.; Hörber, H.; Howard, J.; Müller, D. J. Assembly of Collagen into Microribbons: Effects of pH and Electrolytes. *J. Struct. Biol.* **2004**, *148*, 268-278.

[7] Abrams, G. A.; Goodman, S. L.; Nealey, P. F.; Franco, M.; Murphy, C. J. Nanoscale Topography of the Basement Membrane Underlying the Corneal Epithelium of the Rhesus Macaque. *Cell Tissue Res.* **2000**, *299*, 39-46.

[8] Christman, K. L.; Enriquez-Rios, V. D.; Maynard, H. D. Nanopatterning Proteins and Peptides. *Soft Matter* **2006**, *2*, 928-939.

[9] Falconnet, D.; Csucs, G.; Grandin, H. M.; Textor, M. Surface Engineering Approaches to Micropattern Surfaces for Cell-based Assays. *Biomaterials* **2006**, *27*, 3044-3063.

[10] Arnold, M.; Schwieder, M.; Blümmel, J.; Cavalcanti-Adam, E. A.; López-Garcia, M.; Kessler, H.; Geiger, B.; Spatz, J. P. Cell interactions with hierarchically structured nano-patterned adhesive surface. *Soft Matter*. **2009**, *5*, 72-77.

[11] Malmström, J.; Christensen, B.; Jakobsen, H. P.; Lovmand, J.; Foldbjerg, R.; Sorensen, E. S.; Sutherland, D. S. Large area protein patterning reveals nanoscale control of focal adhesion development. *Nano Lett.* **2010**, 10, 686-694.

[12] Deeg, J. A.; Louban, I.; Aydin, D.; Selhuber-Unkel, C.; Kessler, H.; Spatz, J. P. Impact of local versus global ligand density on cellular adhesion. *Nano Lett.* **2011**, *11*, 1469-1476.

[13] Rolland, O.; Turrin, C.-O.; Caminade, A.-M.;Majoral, J.P. Dendrimers and nanomedicine: multivalency in action. *New J. Chem.* **2009**, *33*, 1809-1824.

[14] Saovapakhiran, A.; D'Emanuele, A. Attwood, D.; Penny, J. Surface modification of PAMAM dendrimers modulates the mechanism of cellular internalization. *Bioconjugate Chem.* **2009**, *20*, 693-701.

[15] Albertazzi, L.; Fernandez-Villamarin, M.; Riguera, R.; Fernandez-Megia, E. Peripheral functionalization of dendrimers regulates internalization and intracelular trafficking in living cells. *Bioconjugate Chem*. **2012**, *23*, 1059-1068.

[16] Mikhail, A. S.; Jones, K. S.; Sheardown, H. Dendrimer-grafted cell adhesion peptide-modified PDMS. *Biotechnol. Prog*. **2008**, *24*, 938-944.

[17] Kino-oka, M.; Kim, J.; Kurisaka, K.; Kim, M.-H. Preferential growth of skeletal myoblasts and fibroblasts in co-culture on a dendrimer-immobilized surface. *J. Biosci. Bioeng.* **2013**, *115*, 96-99.

[18] Lomba, M.; Oriol, L.; Sánchez-Somolinos, C.; Grazú, V.; Moros, M.; Serrano, J. L.; Martínez De la Fuente, J. Cell adhesión on surface patterns generated by the photocrosslinking of hyperbranched polyesters with a trisdiazonium salt. *React. Funct. Polym*. **2013**, *73*, 499-507.

[19] Kim, M. –H.; Kino-oka, M.; Morinaga, Y.; Sawada, Y.; Kawase, M.; Yagi, K.; Taya, M. Morphological regulation and aggregate formation of rabbit chondrocytes on dendrimer-immobilized surfaces with D-glucose display. *J. Biosci. Bioeng.* **2009**, *107*, 196-205.

[20] Kim, M. –H.; Kino-oka, M.; Kawase, M.; Yagi, K.; Taya, M. Synergistic effect of D-glucose and epidermal growth factor display on dynamic behaviors of human epitelial cells. J. Biosci. Bioeng. 2007, 104, 428-431.

[21] Maheshwari, G.; Brown, G.; Lauffenburger, D. A.; Wells, A.; Griffith, L. G. Cell adhesion and motility depend on nanoscale RGD clutering. J. Cell Sci. 2000, 113, 1677-1686.

[22] Pericet-Camara, R.; Cahill, B. P.; Papastavrou, G.; Borkovec, M. Nano-patterning of Solid Substrates by Adsorbed Dendrimers Chem. Commun. 2007, 3, 266-268.
[23] Tokuhisa, H.; Zhao, M.; Baker, L. A.; Phan, V. T.; Dermody, D. L.; Garcia, M. E.; Peez, R. F.; Crooks, R. M.; Mayer, T. M. Preparation and characterization of dendrimer monolayers and dendrimer-alkanethiol mixed monolayers adsorbed to gold. J. Am. Chem. Soc. 1998, 120, 4492-4501.
[24] Pericet-Camara, R.; Papastavrou, G.; Borkovec, M. Atomic force microscopy study of the adsorption and electrostatic self-organization of poly(amidoamine) dendrimers on mica. Langmuir, 2004, 20, 3264-3270.
[25] Li, J.; Piehler, L. T.; Qin, D.; Baker, J. R.; Tomalia, D. A. Visualization and characterization of poly(amidoamine) dendrimers by atomic force microscopy. Langmuir, 2000, 16, 5613-5616.
[26] Mertz, L.; Hitz, J.; Hubler, U.; Weyermann, P.; Diederich, F.; Murer, P.; Seebach, D.; Widmer, I.; Stöhr, M.; Güntherodt, H. –J. STM investigation on single, physisorbed dendrimers. Single Mol. 2002, 5, 295-299.
[27] Horcas, I.; Fernández, R.; Gómez-Rodríguez, J. M.; Colchero, J.; Gómez-Herrero, J.; Baro, A. M. WSXM: A Software for Scanning Probe Microscopy and a Tool for Nanotechnology. Rev. Sci. Instrum. 2007, 78, 13705-13713.
[28] Prats-Alfonso, E.; García-Martín, F.; Bayo, N.; Cruz, L. J.; Pla-Roca, M.; Samitier, J.; Errachid, A.; Albericio, F. Facile Solid-phase Synthesis of Biotinylated Alkyl Thiols. Tetrahedron 2006, 62, 6876-6881.
[29] Boas, U.; Heegaard, P. M. H. Dendrimers in Drug Research. Chem. Soc. Rev. 2004, 33, 43-63.
[30] Zhou, M.; Bentley, D.; Ghosh, I. Helical Supramolecules and Fibers Utilizing Leucine Zipper-Displaying Dendrimers. J. Am. Chem. Soc. 2004, 126, 734-735.
[31] Zhou, M.; Ghosh, I.; Noncovalent Multivalent Assembly of Jun Peptides on a Leucine Zipper Dendrimer Displaying Fos Peptides. Org. Lett. 2004, 20, 3561-3564.
[32] Huang, J.; Gräter, S. V.; Corbellini, F.; Rinck, S.; Bock, E.; Kemkemer, R.; Kessler, H.; Ding, J.; Spatz, J. P. Impact of order and disorder in RGD nanopatterns on cell adhesion. Nano Lett. 2009, 9, 1111-1116.
[33] Xiong, J-P.; Stehle, T.; Zhang, R.; Joachimiak, A.; Frech, M.; Goodman, S. L.; Arnaout, M. A. Crystal Structure of the Extracellular Segment of Integrin αVβ3 in Complex with an Arg-Gly-Asp Ligand. Science 2002, 296, 151-155.
[34] Arnold, M.; Cavalcanti-Adam, E. A.; Glass, R.; Blümmel, J.; Eck, W.; Kantlehner, M.; Kessler, H.; Spatz, J. P. Activation of integrin function by nanopatterned adhesive interfaces. ChemPhysChem. 2004, 5, 383-388.
[35] Liu, L.; Chen, S.; Giachelli, C. M.; Ratner, B. D.; Jiang, S. Controlling Osteopontin Orientation on Surfaces to Modulate Endothelial Cell Adhesion. J. Biomed. Mater. Res. 2005, 74A, 23-31.
[36] Tatkiewicz, W. I.; Seras-Franzoso, J.; García-Fruitós, E.; Vazquez, E.; Ventosa, N.; Peebo, K.; Ratera, I.; Villaverde, A.; Veciana, J. Two-dimensional microscale engineering of protein-based nanoparticles for cell guidance. ACS Nano 2013, 7, 4774-4784.
[37] Lehnert, D.; Wehrle-Haller, B.; David, C.; Welland, U.; Ballestrem, C.; Imhol, B. A.; Bastmeyer, M. Cell behavior on micropatterned substrata: limits of extracellular matrix geometry for spreading and adhesion. J. Cell Sci. 2004, 117, 41-52.
[38] Schaller, M. D. Paxillin: a Focal Adhesion-associated Adaptor Protein. Oncogene 2001, 20, 6459-6472.
[39] Cavalcanti-Adam, E. A.; Volberg, T.; Micoulet, A.; Kessler, H.; Geiger, B.; Spatz, J. P. Cell Spreading and Focal Adhesion Dynamics Are Regulated by Spacing of Integrin Ligands. Biophys. J. 2007, 92, 2964-2974.
[40] Irvine, D. J.; Hue, K-A.; Mayes, A. M.; Griffith, L. G. Simulations of Cell-Surface Integrin Binding to Nanoscale-Clustered Adhesion Ligands. Biophys. J. 2002, 82, 120-132.
[41] Comisar, W. A.; Mooney, D. J.; Linderman, J. J. Integrin organization: linking adhesion ligand nanopatterns with altered cell responses. J. Theor. Biol. 2011, 274, 120-130.

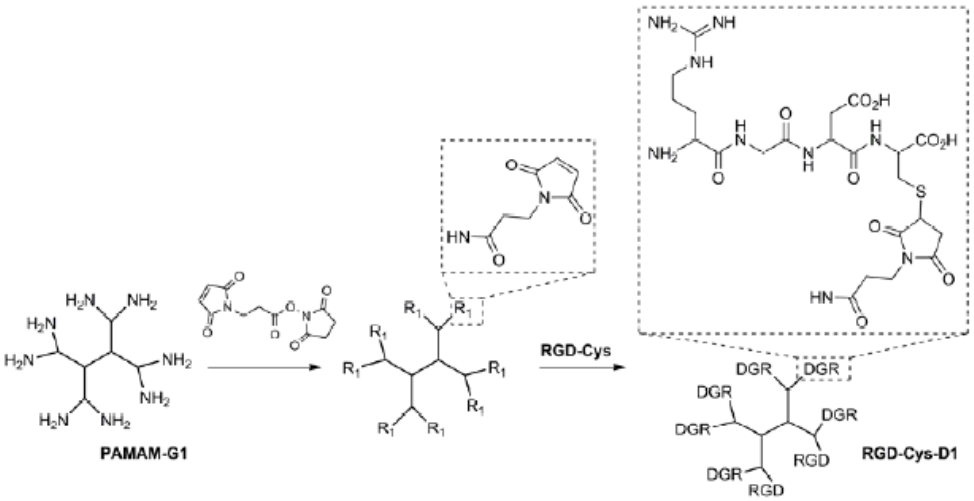

Scheme 1 Synthesis of RGD-Cys-D1 from PAMAM G1.

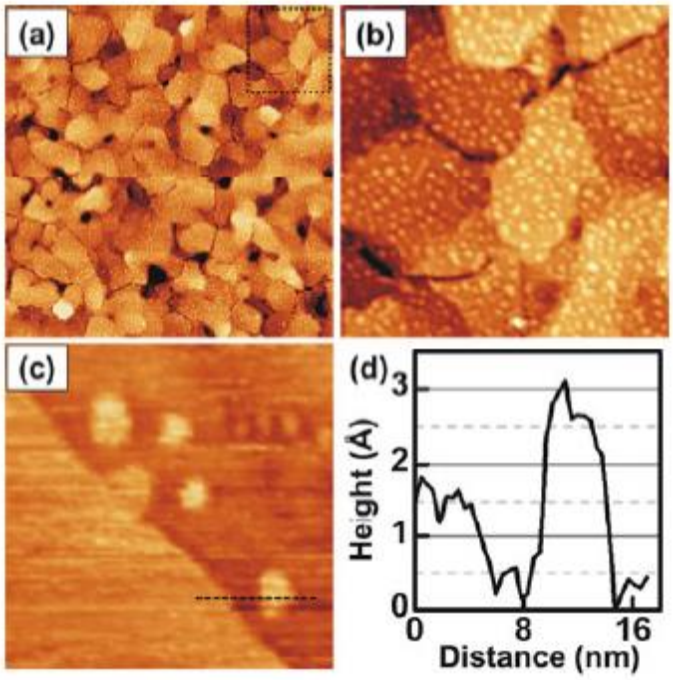

Figure 1 Surface characterization of RGD-Cys-D1 dendrimer nanopatterns on Au(111) with AFM and STM in air. (a) 5x5 μm representative AFM image obtained when patterning was conducted from a bulk concentration of 10^{-5}% w/w. (b) zoom-in from the dashed region in (a). (c) STM image obtained on nanopatterns from an initial bulk concentration of 10^{-8}% w/w (45x45 nm, Bias = 200 mV, Set point = 0.5 nA) and (d) height-distance profile obtained on the dashed region indicated in (c).

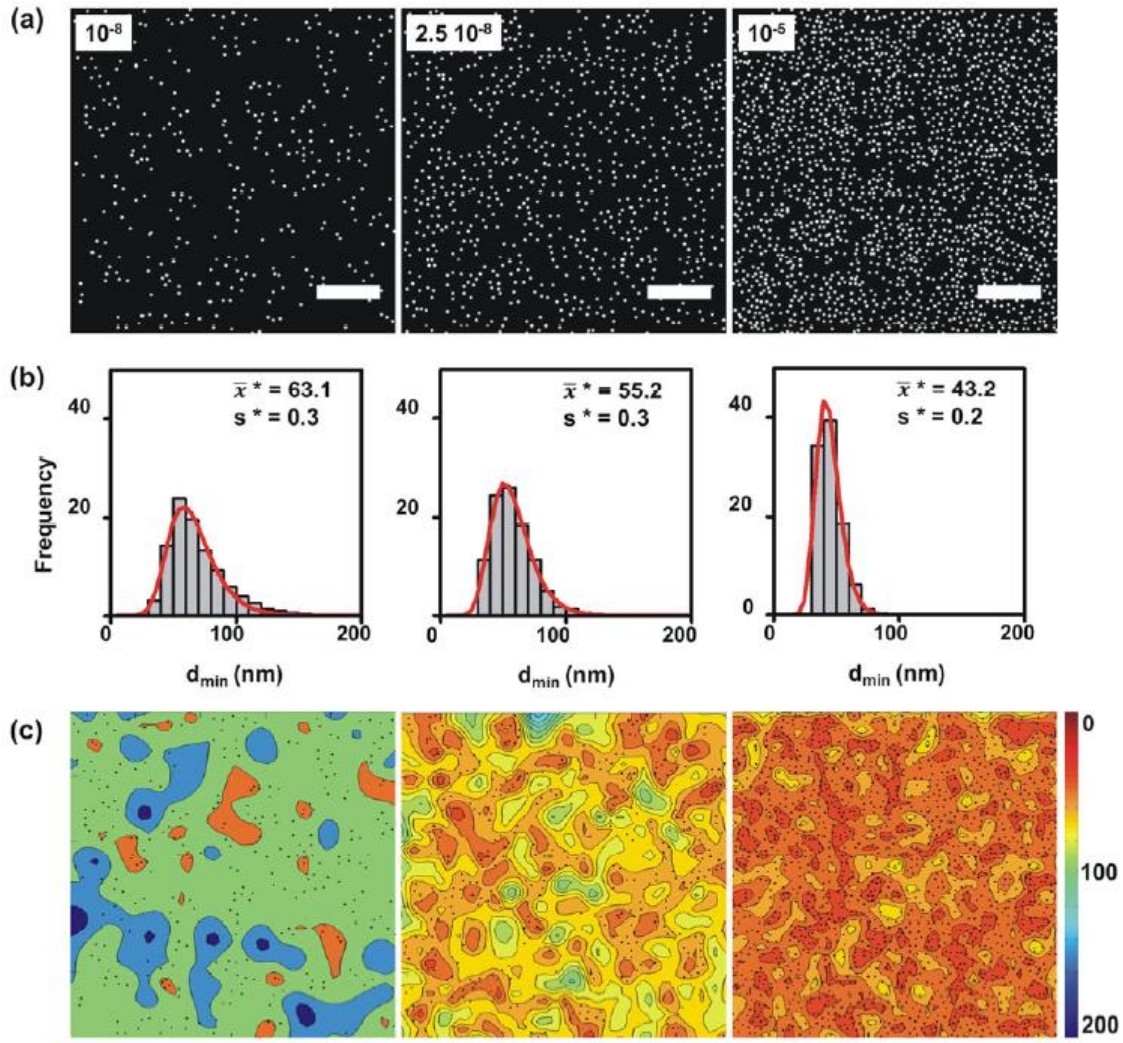

Figure 2 Nanopatterning of RGD-Cys-D1 on Au(111) surfaces. (a) Representative AFM image thresholds obtained from 10^{-8}, 2.5 10^{-8}, and 10^{-5} % w/w RGD-Cys-D1 bulk concentrations. Scale bar = 500 nm. (b) Minimum inter-particle distance (d_{min}) distributions. 63.1, 55.2 and 43.2 nm are the mean values of the shown distributions (s* stand for the standard deviation). The calculated mínimum inter-particle distances for the corresponding ordered patterns are 117, 97, and 66 nm, respectively (c) Corresponding d_{min} probability contour plots obtained from images in (a) (superimposed). Color scale corresponds to d_{min} values in nanometers.

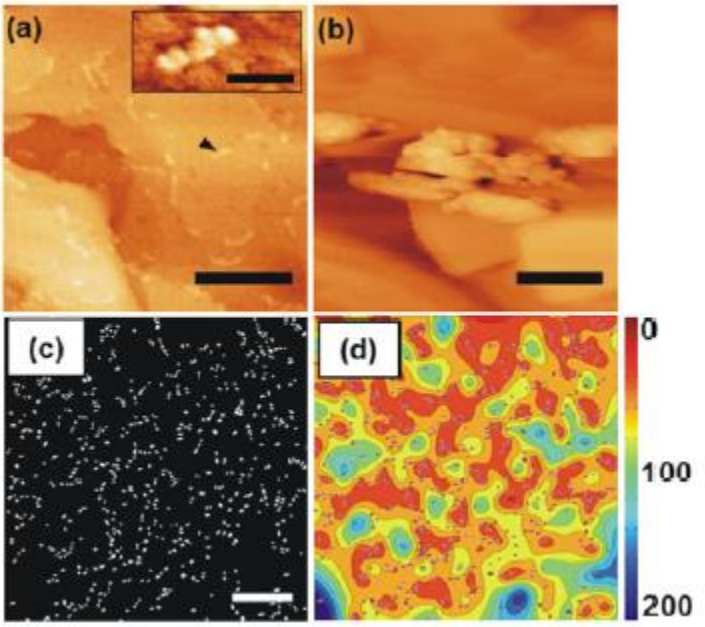

Figure 3 RGD-Cys-D1 nanopatterning on Au(111) surfaces from 10^{-2}% w/w bulk concentration. (a) AFM tapping image (scale bar = 250 nm) showing the presence of dendrimer aggregates. The inset corresponds to the magnified phase image of one of the aggregates (scale bar = 50 nm). (b) High magnification image of aggregates obtained by STM (scale bar = 50 nm). (c) AFM image threshold, scale bar = 500 nm and (d) the corresponding d_{min} probability contour plot. Aggregates are superimposed in dark red pointing out that they are points of high ligand density. Color scale corresponds to d_{min} values in nanometers. The calculated percentage of dense areas with particles (dendrimer aggregates) separated less than 70 nm is 28%.

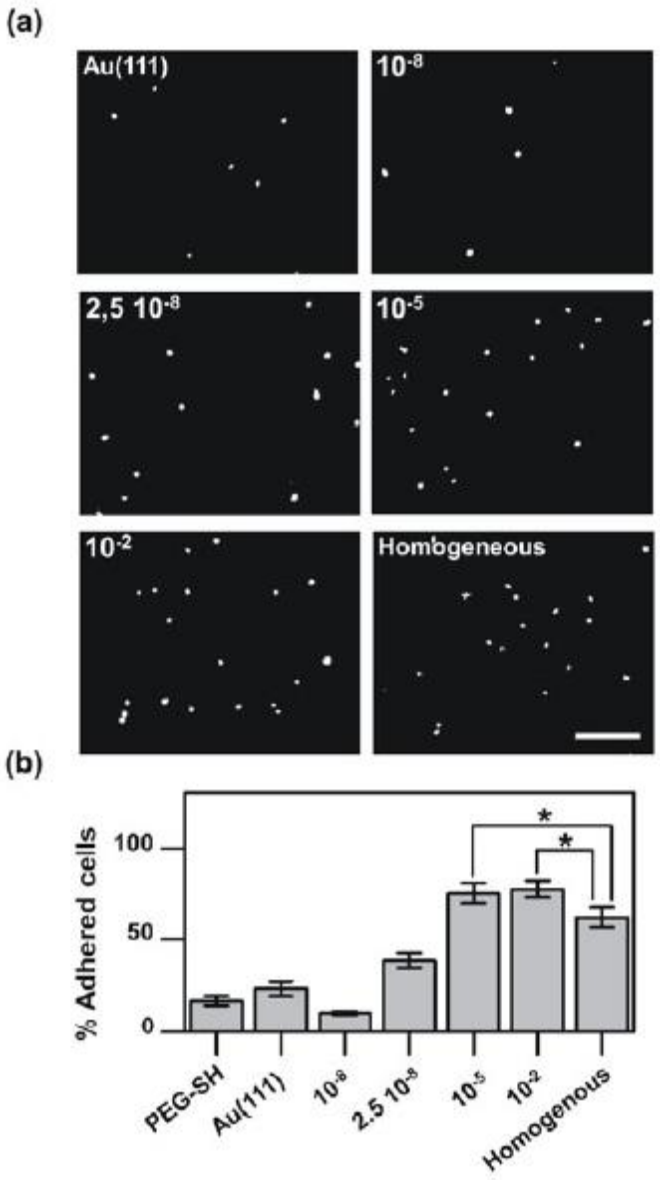

Figure 4 Cell adhesion on RGD-Cys-D1 nanopatterned Au(111) substrates after 4.5 h incubation with a range of bulk concentrations compared with that achieved on Au(111) and homogeneously modified surfaces. (a) Representative fluorescent microscopy images of cell nuclei stained with Hoechst. Scale bar = 200 μm. (b) Percentage of adhered cells presented as the mean with the standard error.

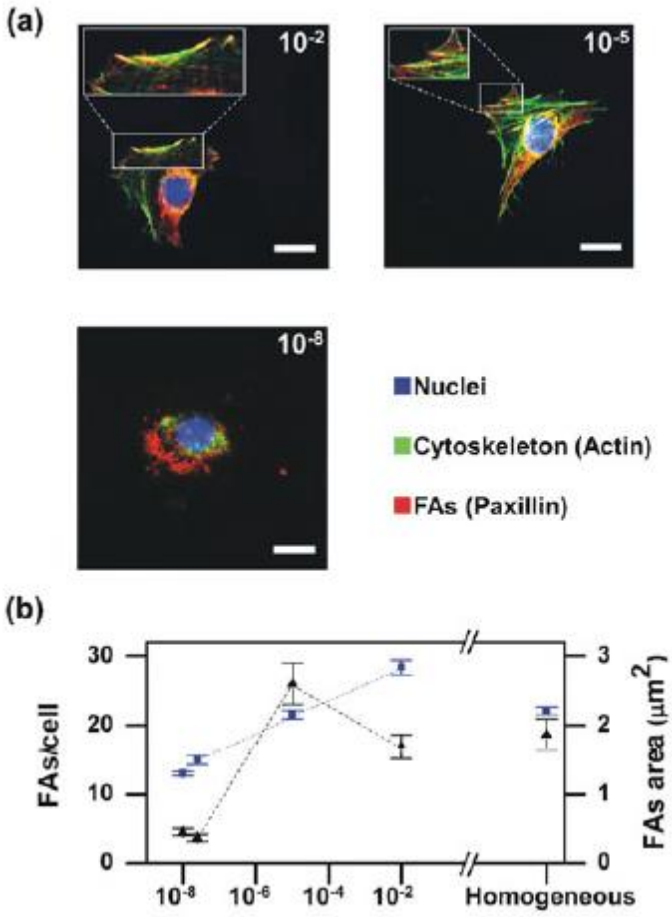

Figure 5 (a) Fluorescent micrographs of representative cells after 4.5 h in culture on the corresponding substrates. Insets show the magnified portion of FAs formed at the cell periphery. Scale bar = 20 μm. (b) Plot of the number of FAs per cell (black triangles) and FA area (blue squares) obtained from various bulk concentrations (logarithmic scale) and from the homogeneous surface (FAs were considered from 1 μm2. The error bars correspond to the standard errors of the mean. Dashed lines are eye guides).